Structural study of the Sn/Ge interface of highly milled Sn-Ge powders

J. K. D. S. Jayanetti, S. M. Heald, and Z. Tan
Brookhaven National Laboratory, Upton, New York 11973
(Received 10 June 1992; revised manuscript received 9 September 1992)

Structural changes occurring at the Sn/Ge interface of highly milled Sn-Ge powders were examined using extended x-ray-absorption fine-structure spectroscopy (EXAFS). X-ray diffraction and differential scanning calorimetry were also used as supporting techniques. Samples of varying compositions were prepared for analysis. Systematic changes in EXAFS and x-ray diffraction are observed with decreasing Sn concentration. These changes are found to be due to the fact that Sn appears in two different states, i.e., the metallic phase and an α-Sn/Ge alloy phase several monolayers thick that forms at the Sn/Ge interface. When the Sn concentration is 20 vol% the alloy phase becomes the dominant phase, leaving essentially no Sn in the normal β-Sn phase. The results can be used to explain previously observed reductions in melting enthalpy and a low-temperature tail in the melting transition. The thermal stability of the alloy above the melting point of bulk Sn accounts for the reduction in melting enthalpy of Sn, and residual small Sn particles are the likely cause for the low-temperature tail in melting.

I. INTRODUCTION

Recently, Jang and Koch[1,2] have made some interesting observations in x-ray-diffraction (XRD) and differential scanning calorimetry (DSC) studies done on mechanically milled Sn-Ge powders. They have seen the possible depression of melting point and broadening of the melting transition region of Sn with decreasing Sn content. Another observation is the decrease of enthalpy of fusion of the Sn melting transition with decreasing Sn content. This is attributed to the retention of Sn in a disordered state at the Sn/Ge interface. When the Ge particle size reaches a value where essentially all the Sn atoms are adjacent to the Ge particle surfaces, all the Sn is said to be in this disordered state such that no melting transition is observed. Turnbull, Jang, and Koch[3] have suggested a theoretical model which explains the reduction of melting enthalpy of Sn. This model is based on the assumption that Sn is in two states, namely, bulk and interfacial. They have estimated the thickness of this interfacial Sn layer to be about one monolayer. Our objective was to look at this Sn/Ge interface from the structural point of view in order to obtain a clear picture of this behavior. It is known that small amounts of Ge can stabilize the cubic phase of Sn, α-Sn, at temperatures above room temperature.[4] Recent literature also reports the existence of α-Sn/Ge alloys grown using molecular-beam epitaxy on substrates such as Ge, CdTe, and InSb.[5–8] Hochst, Engelhardt, and Hernandez-Calderon[5] have grown α-Sn/Ge alloys epitaxially on Ge(100) substrates at temperatures of about 400 °C. We began our investigation to see whether there is such a phase change or an alloy formation at the Sn/Ge interface using extended x-ray-absorption fine-structure (EXAFS) measurements. EXAFS is a proven tool to study disordered materials because of its ability to investigate the local atomic structure of each of the components in a material. X-ray diffraction and differential scanning calorimetry have also been used to support our results. The objective of this paper is to provide a detailed discussion about the results we have obtained which explains the reduction of melting enthalpy of Sn due to the formation of an α-Sn/Ge alloy at the interface. The alloying of Sn and Ge appears to occur in a different way compared to the conventional mechanical alloying. Milling causes the ductile Sn to form a coating around the brittle Ge particles. The resulting mixing of Sn and Ge at the interface gives rise to alloying that is limited to a thickness of several monolayers around the Ge particles. We have made similar observations of alloying in highly milled Sn-Si powders, which will be discussed in a future paper. In this paper we briefly discuss the experimental procedure in Sec. II. Section III provides a discussion about experimental data, analysis, and how we arrive at our final model based on the experimental data and calculations. Section IV is used to summarize and discuss our results comparing the consistency of results obtained from different techniques, followed by the conclusions.

II. EXPERIMENT

Sn/Ge powder samples were milled using a Brinkmann Model MM2 standard mixer mill operated in an Ar ambient. A SPEX 8000 mixer/mill was also used for some later samples. Powders (-100 mesh, 99.999% pure) were milled in a sealed hardened tool steel vial, using a steel ball. Loading and unloading of powders to the vial and preparation of samples for EXAFS, XRD, and DSC measurements were done inside a dry box with moisture and oxygen content of <5 ppm. Powders with varying Sn/Ge volume ratios (20-, 30-, and 40-vol% Sn) were milled for nearly a constant time of about 35 h.

For differential scanning calorimetry, samples were sealed in aluminum pans. DSC analysis was done using a DuPont 910 DSC system. The sample produced melting enthalpy results (see Table I) similar to those of Jang and Koch. In order to prepare x-ray samples of proper absorption, the powders had to be diluted to proper amounts. We maintained the absorption step $\Delta\mu x$ at the Sn K edge to be approximately 1.5 this way. Initially

samples were diluted with powdered graphite (carbon). Samples were packed in an array of slots made in a rectangular Cu holder and sealed in a copper cell using an indium seal. The cell contained kapton x-ray windows sealed with epoxy. Another sample (20-vol % Sn) was packed in a slotted Al plate using thin Al windows to perform the heating experiments. In a second run, samples were diluted using boron nitride powder, which improved the packing performance and produced EXAFS data of better quality. Because boron nitride is hydroscopic, care was taken to bake the powder in a rough vacuum before mixing with the samples. An attempt was made to make an α-Sn standard by melting a piece of β-Sn (tetragonal or metallic phase) with a very small amount of Ge (<0.5 at. %) in an UHV chamber. In order to initiate the transformation the specimen was kept in a freezer at -30 °C. After two days the sample had transformed. It was ground to a fine powder and rubbed onto kapton tape. EXAFS analysis indicated that some of the powder had transformed back to tetragonal β-Sn during the grinding.

EXAFS measurements were made at beamline X-11A at the National Synchrotron Light Source at Brookhaven National Laboratory. Measurements were made in the transmission mode using a Si(311) double-crystal monochromator. The incident and the transmitted x-ray beams were monitored using Ar and Kr gas filled ionization chambers, respectively. The monochromator entrance slit was maintained at 0.25 mm and the energy resolution at the Sn K edge was estimated to be 6.5 eV. Care was taken to reduce the effects from higher harmonics by detuning the monochromator. Sn K-edge (29 200 eV) EXAFS measurements were made at temperatures of 10, 100, and 200 K, in a rough vacuum. The 20-vol % Sn sample prepared for heating experiments was heated in a vacuum above the Sn melting point and up to about 300 °C while measuring EXAFS at several temperatures.

The diffraction measurements of the samples were made at room temperature at an energy of 8.5 keV. Measurements were done at beamline X-11B using a modified Phillips goniometer with an INEL 120° curved position-sensitive detector. This configuration allowed us to acquire a complete diffraction pattern in about three minutes.

III. DATA AND ANALYSIS

In this section we discuss the major features in our experimental data and the data analysis procedure. Emphasis is given to our main structural probe, the x-ray-absorption fine-structure technique, with a detailed discussion.

X-ray-diffraction data obtained at 8.5 keV show a systematic decrease in the intensity of β-Sn peaks with the decreasing Sn volume percentage (Fig. 1). At 20 vol. % Sn, the Sn peaks have almost disappeared, indicating the Sn is in a different state which is possibly amorphous. Another clear feature is the systematic increase in broadening of the Ge peaks as the volume percentage of Sn is decreased. Diffraction-peak-broadening analyses were carried out on diffraction profiles of the Ge(111)

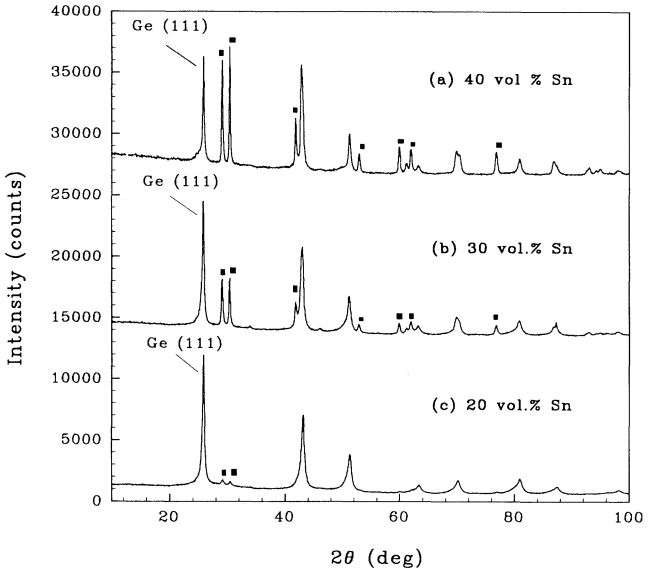

FIG. 1. Room-temperature XRD measurements of (a) 40-vol % Sn, (b) 30-vol % Sn, and (c) 20-vol % Sn taken at 8.5 keV. Peaks marked by a box correspond to β-Sn diffraction profiles.

peak on each sample assuming that the broadening is caused by crystallite size and microstrain. A single-peak analysis method was used, assuming the profile is Voigtian (a convolution of Cauchy and Gaussian).[9] The results are given in Table I.

The EXAFS oscillations are a final-state photoelectron effect arising from interference between the outgoing photoejected electron wave and the backscattered waves from neighboring atomic sites. Using a simple single-scattering parametrization the EXAFS modulations can be written as[10]

$$\chi(k)=\frac{\mu(k)-\mu_0(k)}{\mu_0(k)} = \sum \frac{N_j}{kR_j^2}F_j(k)e^{-2k^2\sigma_j^2}e^{-2R_j/\lambda}\sin[2kR_j+\delta_j(k)] , \quad (1)$$

where $\mu(k)$ is the total absorption coefficient measured

TABLE I. Summary of EXAFS, XRD, and DSC results. The average particle size at each concentration was measured by using the broadening analysis of Ge(111) diffraction profile. The experimentally obtained melting enthalpy of pure Sn is 61.5 J/g. The EXAFS fitting results give the relative amount of Ge and Sn near neighbors present at each concentration.

Vol % of Sn	Average particle size (Å)	Melting enthalpy of Sn (J/g)	Sn-Ge contribution (%)
40	405±155	48.8	16.4
30	300±95	20.0	32.7
20	250±70	3.6	87.5

above the edge and $\mu_0(k)$ is the smoothly varying atomic contribution. The summation is over coordination shells of atoms surrounding the absorbing atom with N_j atoms in shell j situated at an average distance R_j from the central atom. σ_j^2 is the mean-square relative positional displacement of the central and backscattering atoms from both thermal and structural disorder (Debye-Waller factor). The quantity λ is the mean free path that corresponds to a finite lifetime of the excited state, $F_j(k)$ is the backscattering amplitude of the atoms in the jth shell, and $\delta_j(k)$ is the phase shift experienced by the photoelectron as it traverses the potential of the central and backscattering atoms. The variable k is related to the energy E of the incident photon by $k=[2m(E-E_0)/\hbar^2]^{1/2}$, where m is the electron mass and E_0 is the threshold energy.

According to Eq. (1), the resultant EXAFS is a sum of sine waves with periods $2kR_j$ from each shell j with an amplitude which represents the number of neighbors modified by an envelope due to the backscattering amplitude, the Debye-Waller-type damping, and the mean-free-path damping. Therefore EXAFS is able to provide direct, quantitative details of the local atomic environment around each kind of atom, including the type and number N_j of surrounding atoms, their mean distance R_j, and the dynamic (thermal) and static (structural) displacement σ^2 about their average positions, through a proper data analysis.

The data analysis procedure we discuss below was done using the University of Washington EXAFS data analysis software package. The EXAFS data of the Sn K edge were extracted using standard techniques of background subtraction and normalization.[11] The maximum derivative point was chosen to be the edge position E_0 (threshold energy), and the data were normalized to the edge step. For illustration data of 40- and 20-vol % samples are presented since they show contrasting differences. Figure 2 shows the k^2-weighted EXAFS $\chi(k)$ data obtained at 10 K for powder samples of 40- and 20-vol % Sn compared to the EXAFS of β-Sn powder. The corresponding EXAFS radial distribution functions (RDF's) were obtained (Fig. 3) by transforming the k^2-weighted data over a k-space range of 3.4 to 16 Å^{-1}. The 40-vol % Sn RDF data clearly show a new peak P_B which has evolved on the left-hand side of peak P_A which corresponds to the first Sn-Sn nearest neighbors of the β-phase. At this point we identify this new form of Sn to be interfacial Sn, as suggested by Turnbull, Jang, and Koch.[3] At 20 vol % Sn, peak P_A vanishes, leaving only peak P_B, indicating that Sn does not appear to be in the β phase at this concentration. When we measured the EXAFS of the 20-vol % Sn sample as a function of temperature, it was observed that there was essentially no change in EXAFS (Fig. 4) as the sample was heated above the Sn melting point, and the thermal damping was much less than that for β-Sn. A similar observation was made during DSC measurements, when the 20-vol % sample was heated up to 400 °C. A broadened slight dip around the β-Sn melting point was observed. This gave a melting enthalpy of 3.6 J/g (see Table I), corresponding

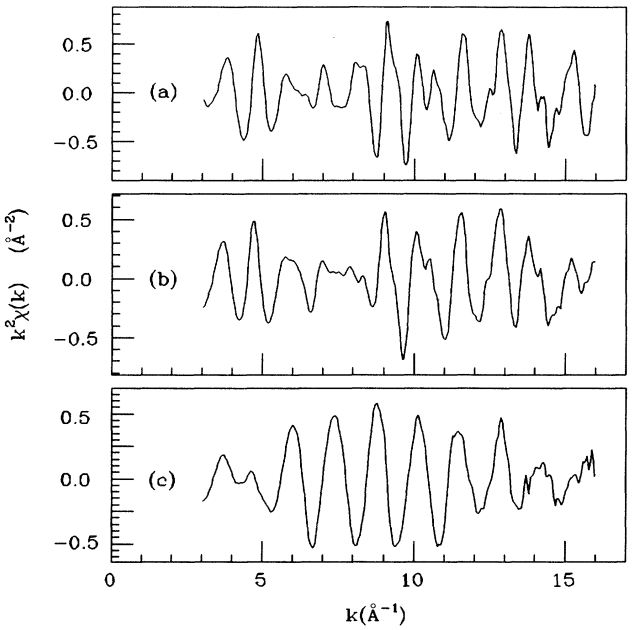

FIG. 2. Background subtracted k^2-weighted EXAFS from the Sn K edge obtained at 10 K for (a) β-Sn powder, (b) 40-vol % Sn, and (c) 20-vol % Sn samples.

to melting of residual β-Sn. There were no further signs of a phase change or a decomposition below 400 °C. This indicates that this interfacial Sn phase is stable at higher temperatures.

In order to further look at this interfacial Sn form we followed the procedure discussed below. The contamina-

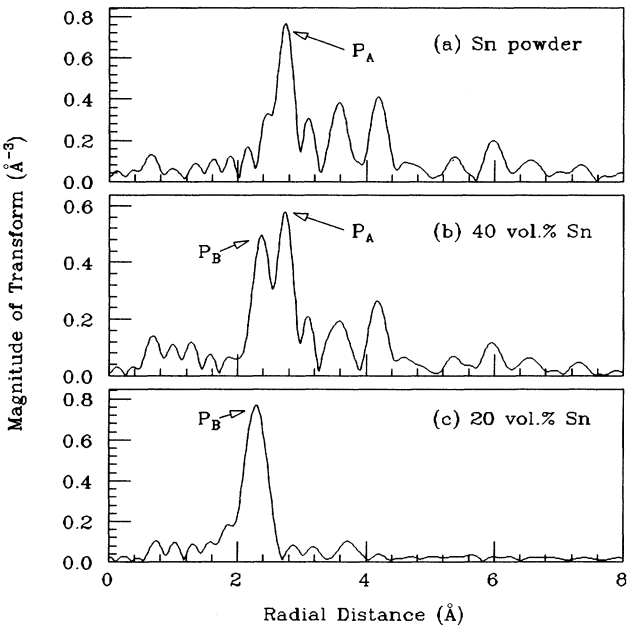

FIG. 3. Fourier transforms of EXAFS $k^2\chi(k)$ data (10 K) from the Sn K edge in (a) Sn powder, (b) 40-vol % Sn, and (c) 20-vol % Sn.

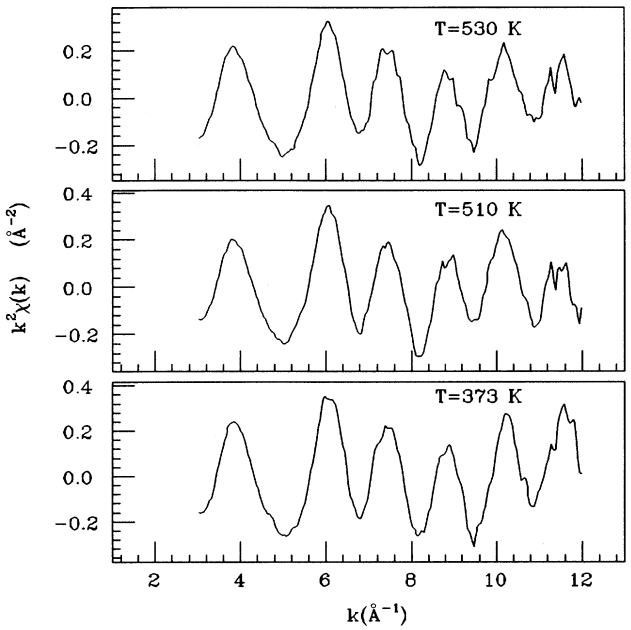

FIG. 4. $k^2\chi(k)$ of 20-vol % Sn sample measured at $T=373$, 510, and 530 K.

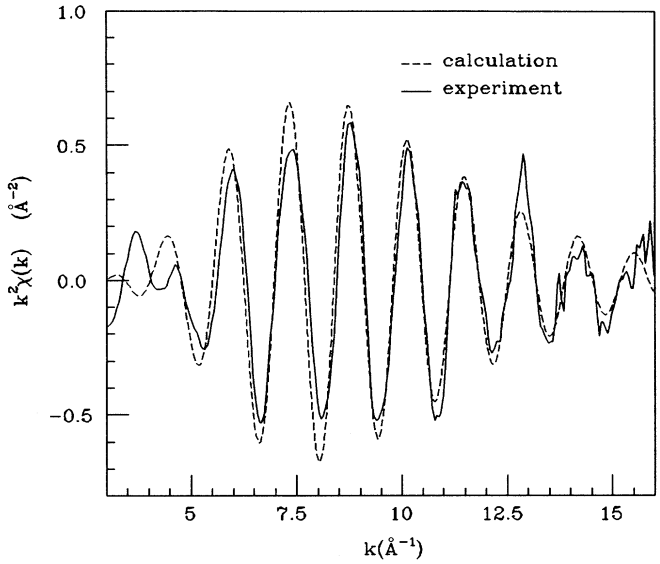

FIG. 5. $k^2\chi(k)$ of 20-vol % Sn sample (solid line) compared to the first shell $k^2\chi(k)$ of the calculated ordered 50-at. % α-Sn/Ge alloy (dashed line).

tion of the α-Sn standard by β-Sn made it difficult to use during our analysis. Therefore the first-shell EXAFS due to α-Sn was calculated using the FEFF theoretical code (Version 4.08), which takes into account the curved wave nature of the photoelectron.[12] The program requires the many-body correction parameter S_0^2, which accounts for the reduction of EXAFS amplitude, as an input. This was adjusted by comparing the calculation to the experimental data of β-Sn powder. A value of 0.85 was found to be reasonable. We also used FEFF theoretical code to calculate the first-near-neighbor EXAFS from a 50-at. % α-Sn/Ge alloy using two approaches. One approach was to use a 50-at. % α-Sn/Ge alloy with a Sn atom surrounded by four Ge atoms in a chemically ordered zinc-blende structure. The second approach was to assume a Sn atom to be surrounded by two Ge atoms and two Sn atoms so that the 50:50 atomic ratio is preserved whereas the chemical environment could be random. In both cases the first-near-neighbor distance of 2.62 Å was used in calculations, by assuming the lattice parameter of the alloy (6.06 Å) to have the average value of the lattice parameters of α-Sn and Ge (6.46 and 5.65 Å, respectively[13]). Figure 5 shows the comparison of k^2-weighted EXAFS $\chi(k)$ of the 20-vol % Sn sample and the calculated ordered 50-at. % α-Sn/Ge alloy. The two spectra are in very close agreement with each other, indicating that the 20-vol % Sn sample spectrum is essentially due to single-shell EXAFS of Sn-Ge first near neighbors.

In order to extract parameters such as the Debye-Waller factor, coordination number, and distance, the 20-vol % Sn RDF peak in R space was back-transformed to k space using a suitable R-space window. Then a least-squares fitting method was used to adjust the parameters relative to the appropriate standards. The standards used for fitting were the calculated first-shell EXAFS ordered 50-at % α-Sn/Ge alloy, the calculated first-shell EXAFS of α-Sn, and the measured EXAFS of the β-Sn powder. The latter standards α-Sn and β-Sn were used to see whether the 20-vol % Sn sample is actually multicomponent due to small contributions from α-Sn and β-Sn which are hidden in the single-shell-like sample RDF peak. For the sample and standards an R-space window between 1.5 and 3.4 Å was chosen for filtering so that it includes the peak of interest while not interfering with the peaks due to other shells. The upper limit (3.4 Å) was determined by the β-Sn powder. β-Sn has two close first and second shells in the structure which are difficult to isolate by filtering, and the filtering, window was chosen to include both shells. Prior to fitting, the experimental $\chi(k)$ were corrected using McMaster coefficients[14] to account for the falloff of $\mu_0(k)$ past the edge. The amplitude correction at high k (at 16 Å^{-1}) was found to be about 9%.

Fitting for the 20-vol % Sn sample was attempted using two different models. One was to use a single-shell model where first-shell EXAFS is assumed to have only Sn-Ge near neighbors. The fitting parameters were the three floating variables N, R, and σ^2 for Sn-Ge neighbors and the discrete variable E_0. The E_0 adjustment was found to be significant, especially when fitting theoretical standard with the experimental data (see Table II). Fitting was tested using this model for the first-shell EXAFS of the sample obtained at three different temperatures. This way we can achieve a higher accuracy in the coordination number by minimizing the uncertainty arising due to its correlation with the Debye-Waller factor. This model agrees quite well with the experiment, indicating that the Sn RDF peak is due to Sn-Ge first near neighbors. However, the experimental data from XRD (Fig. 1) and DSC (Table I) show that there is a small amount of

TABLE II. EXAFS fitting results obtained for (a) 20-vol % Sn and (b) 30- and 40-vol % Sn. For 20-vol % Sn sample results obtained using both models are reported. In the two-shell model the fitting result for $N_{\text{Sn-Sn}}$ approaches zero at 120 and 200 K.

(a) 20-vol % Sn

(1) Single-shell model

Temperature (K)	$N_{\text{Sn-Ge}}$	$\Delta\sigma^2$ (Å)	$R_{\text{Sn-Ge}}$ (Å)	E_0 (eV)
10	2.48±0.40	0.0031±0.0009	2.64±0.03	−5.5
120	2.52±0.40	0.0038±0.0010	2.64±0.03	−5.5
200	2.48±0.40	0.0043±0.0012	2.64±0.03	−5.5

(2) Two-shell model

Temperature (K)	$N_{\text{Sn-Ge}}$	$N_{\text{Sn-Sn}}$	$\Delta\sigma^2$ (Å^2)	$R_{\text{Sn-Ge}}$ (Å)	E_0 (eV)
10	2.56±0.44	0.36±0.48(−0.36)	0.0034±0.0015	2.64±0.03	−5.5

(b) 30- and 40-vol % Sn

	30-vol % Sn		40-vol % Sn	
Temperature (K)	$N_{\text{Sn-Ge}}$	$N_{\text{Sn-Sn}}$	$N_{\text{Sn-Ge}}$	$N_{\text{Sn-Sn}}$
10	2.2±0.40	2.7±0.60	1.4±0.40	4.8±0.60

β-Sn present at this concentration. Therefore in the second model fitting was tried using both Sn-Ge and Sn-Sn bonds. During fitting, sample Sn-Sn neighbors were assumed to have the same bond distance and σ^2 as in the bulk Sn powder. The only additional variable floated during fitting was the number of Sn-Sn bonds relative to the standard, which has six. This two-shell model lowered the least-squares fitting minimum by approximately 20% and improved the fit at low k. The fitting result obtained at 10 K is illustrated in Fig. 6. The fitting parameters obtained at each temperature, using both models, are given in Table II. For the two-shell fits at 120 and 200 K, the amount of β-Sn near neighbors approaches zero. A possible explanation for this inconsistency is shown in Fig. 7, which compares the temperature-dependent (filtered in the range 1.5–3.4 Å) k^2-weighted $\chi(k)$ of β-Sn to that of the 20-vol % Sn sample. The relatively high amplitude reduction (higher Debye-Waller factor) of β-Sn at higher temperatures makes its presence less significant during fitting. Even

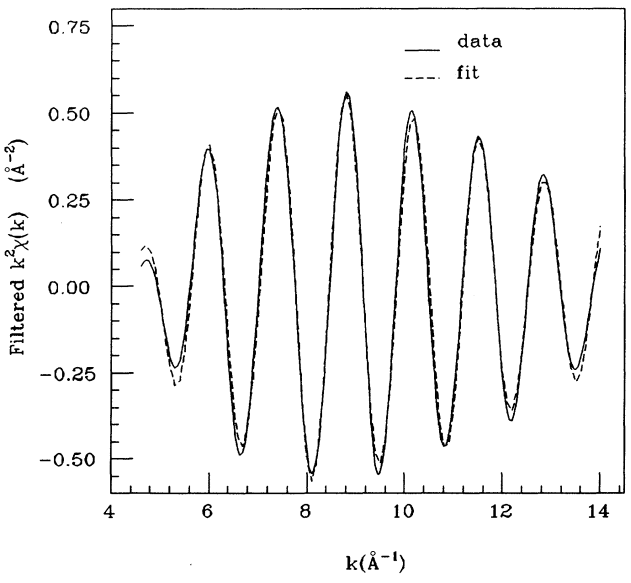

FIG. 6. Comparison of filtered $k^2\chi(k)$ of 20-vol % Sn sample data (solid line) to the two-shell model fit (dashed line).

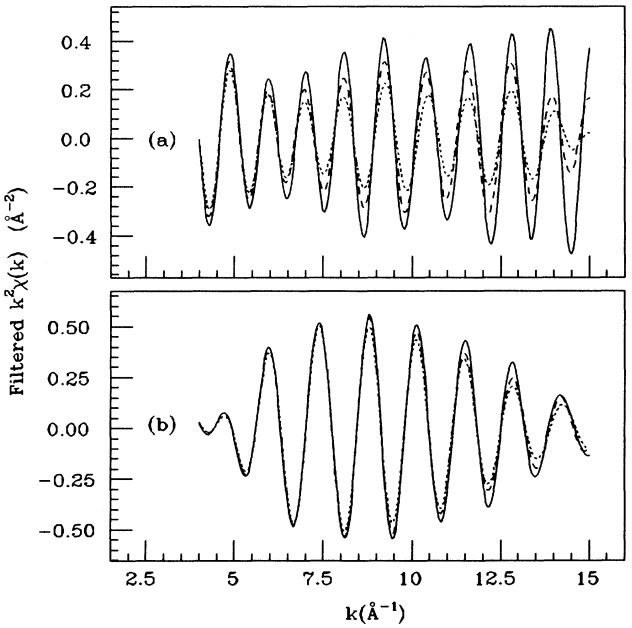

FIG. 7. Comparison of filtered $k^2\chi(k)$ of (b) 20-vol % Sn sample to that of (a) Sn powder at 10 K (solid line), 120 K (dashed line), and 200 K (dotted line).

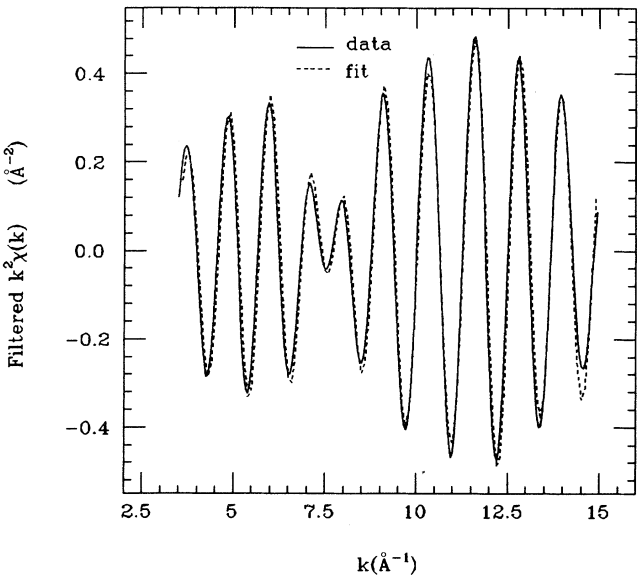

FIG. 8. Comparison of filtered $k^2\chi(k)$ of 40-vol % sample data (solid line) to the fit (dashed line).

though the error bar makes the EXAFS result for the inclusion of β-Sn ambiguous, the XRD and DSC data made us reach the conclusion that the 20-vol % Sn sample must have a small amount of β-Sn quantitatively represented by our result. However, both models clearly show that the major contribution to the EXAFS at this concentration comes from Ge near neighbors which participate in bonding with Sn. In each of these cases the average Sn-Ge first-near-neighbor distance was found to be 2.64±0.02 Å, which gives a value of 6.10±0.05 Å as the lattice parameter of the alloy phase. Fits were also made and preliminary results were reported[15] including a small α-Sn contribution. However, the small improvement obtained did not justify its inclusion.

Quantitative information about the alloy and β-Sn phases at higher Sn concentrations were obtained using the data from the β-Sn powder (for Sn-Sn pairs) and the 20-vol % Sn (for Sn-Ge pairs) as standards during fitting. This way, the number of Sn-Ge bonds could be estimated with respect to the fitting result (2.56 Sn-Ge bonds per Sn atom) obtained for the 20-vol % Sn sample. Data and standards were back-transformed to k space using the same R-space window of 1.5–3.4 Å. Figure 8 gives an illustration of the fitting results we obtained at 10 K for 40-vol % Sn using this method. The results indicate that the samples can be described as a mixture of β-Sn and the interfacial phase. The amount of β-Sn present in the 20-vol % Sn sample was taken into consideration when obtaining the final result (see Table II).

IV. RESULTS AND DISCUSSION

According to Table II, EXAFS results obtained for the 20-vol % Sn sample show a reduction of the number of Ge near neighbors by about 35% as compared to the expected value of four neighbors. However, as discussed above, the closest representative is the calculated EXAFS due to four Ge near neighbors. Replacement of one Ge neighbor by Sn will add a sidelobe to the single Sn-Ge RDF peak and disagrees with 20-vol % RDF. Our interpretation for this result is the following. As explained by Turnbull's model, Sn coats the Ge particles to a certain thickness, but forms an alloy with Ge around the Ge core particles instead of existing as pure Sn in a disordered form. As shown below, this alloy layer is thin and it is likely that the outermost Sn atoms are not fully coordinated. In addition, disorder in this alloy layer could also be contributing to the lowering of the coordination.

Table I shows a summary of results that we gathered using the EXAFS, XRD, and the DSC analysis. As observed previously by Jang and co-workers, the melting enthalpy of Sn decreases with decreasing Sn concentration. EXAFS results in column 4 show the percentage of α-Sn/Ge alloy present at each concentration. Decreasing amounts of β phase are observed as the Sn concentration is decreased, leaving the alloy to be the dominant phase. The observed temperature stability of this phase accounts for the reduction of melting enthalpy. The DSC analysis showed that this phase is stable at least up to 400 °C. As illustrated in Fig. 7, the smaller thermal damping of the 20-vol % Sn sample (which mainly contains the alloy phase) compared to that of β-Sn powder is another sign that this phase has stronger bonds. It has been shown that the thermal vibrations of the first near neighbors can well be represented by the Einstein model.[16,17] Therefore, the Einstein temperature for the Sn-Ge bonds in the 20-vol % sample was determined. The determined value 268±11 K is in the range of Einstein temperatures found[18] for the tetrahedral semiconductors such as Ge (352 K), GaAs (318 K), and ZnSe (269 K) and is much higher than metallic Sn (150 K).[19]

Column 2 in Table I shows the average particle size of Ge at each concentration obtained by XRD line-shape analysis. The particle size decreases with the decreasing concentration irrespective of the fact that all the samples were milled essentially for the same time. A possible explanation for this behavior is the ductile nature of metallic Sn, which acts as a barrier during milling by preventing Ge from further cleavage. We used the particle size and EXAFS results together for the estimation of the volume ratio of the alloy phase to excessive Ge (Ge which does not participate in bonding with Sn). The Ge core particles were assumed to be covered uniformly by this 50-at. % alloy layer to a certain thickness. In order to estimate the thickness of this interfacial alloy layer we used the same assumption as Turnbull, Jang, and Koch.[3] The Ge particles were assumed to have cubic shapes with their average diagonal size being represented by the particle size measurements obtained by XRD. The estimated thicknesses are given in Table III. At each concentration the results are consistent with the Ge particles being covered by an alloy layer of almost constant thickness of about 9 Å (approximately four monolayers). Even though the TEM studies show that the Ge core particles predominantly resemble cubic shapes, layer thicknesses were estimated assuming spherical shapes also. The obtained average alloy layer thickness is about 15 Å. Ac-

TABLE III. Estimated thicknesses of the interfacial α-Sn/Ge alloy layer at each Sn concentration. The alloy was assumed to be 50 at. % and the Ge particles were assumed to have (a) cubic geometry with the dimension across the cube diagonal and (b) spherical geometry with the dimension across the diameter of the sphere, represented by the particle size determined by XRD.

Vol % of Sn	Vol. ratio of $Sn_{0.5}Ge_{0.5}$/unbonded Ge (%)	Thickness of $Sn_{0.5}Ge_{0.5}$ interfacial layer (Å) (a) cubic geometry	(b) spherical geometry
40	22.1	8.0	13.9
30	28.4	7.5	13.0
20	51.0	10.6	18.4

cording to our result the reaction at the interface includes several monolayers, in contrast to the model of Turnbull, Jang, and Koch, which assumes the existence of a single monolayer of disordered Sn at the interface. The decreasing particle size makes more interfacial area available for alloying. The consistency of the results indicates that the assumption of the 50/50 atomic composition for alloy is reasonable. This is also supported by the fact that the α-Sn/Ge alloys epitaxially grown on Ge(100) substrates have a preferred composition of approximately 50 at. %.[5] Further, Bowman *et al.*[7] have estimated the lattice parameters of α-Sn/Ge alloys grown epitaxially on CdTe substates, for lower Ge concentrations. The variation of lattice constant with the atomic concentration seems to follow a linear relationship. Extrapolation of these results gives a value of 6.15 Å for the lattice constant of a 50-at. % α-Sn/Ge alloy, which is in good agreement with our result.

An interesting question is whether this alloying plays any role in the depression of the melting point of Sn and broadening of the melting transition in these samples. The present work does not give direct answers to this question. Koch, Jang, and Gross[1] claim the increasing interfacial area formed during milling to be the cause of melting point depression of Sn. However, another explanation is the previously observed particle size effect on the melting temperature of Sn. There are several articles[20–22] which explain the melting point depression observed for small particles of Sn, Au, Pb, and Bi, in terms of the particle size. Wronsky[20] and Tagaki[20] have done interesting studies on the size dependence of the melting point of small particles of Sn. Decreasing particle size is shown to lower the Sn melting point. When particles are about 100 Å in size the associated melting point depression is found to be about 25 °C, which is in the range of the depression observed by Koch, Jang, and Gross.[1] In our case the residual Sn (any Sn particle not participating in bonding with Ge) can be assumed to have a size distribution similar to the Ge particles. Thus the simplest explanation is that small Sn particles are the cause of the melting point depression of Sn in these samples.

To summarize, based on our experimental results, the disorder at the Sn/Ge interface occurs due to the formation of α-Sn/Ge alloy several monolayers thick. The observed stability of this alloy above the melting point of bulk Sn explains the behavior of melting enthalpy of Sn with the decreasing Sn content. The increasing interfacial area increases the amount of alloy formed. Even though this work does not directly explain the observed melting point depression of Sn, the particle size effect is the likely cause.

ACKNOWLEDGMENTS

We would like to thank Dr. C. K. Saw of Hoechst-Celanese and Dr. S. S. Prasad of Moltech Corp. for their help with various parts of this experiment. This work is supported by the U.S. Department of Energy, Division of Material under Contract No. DE-AC02-76CH00016. The X-11 beamlines are also supported by the DOE Division of Material under Contract No. DE-AS05-80-ER10742.

[1] C. C. Koch, J. S. C. Jang, and S. S. Gross, J. Mater. Res. **4**, 557 (1989).
[2] J. S. C. Jang and C. C. Koch, J. Mater. Res. **5**, 325 (1990).
[3] D. Turnbull, J. S. C. Jang, and C. C. Koch, J. Mater. Res. **5**, 1731 (1990).
[4] A. W. Ewald, J. Appl. Phys. **22**, 1436 (1954).
[5] H. Hochst, M. A. Engelhardt, and I. Hernandez-Calderon, Phys. Rev. B **40**, 9703 (1989).
[6] M. T. Asom, E. A. Fitzgerald, A. R. Kortan, B. Spear, and L. C. Kimerling, Appl. Phys. Lett. **55**, 578 (1989).
[7] R. C. Bowman, Jr., P. M. Adams, M. A. Engelhardt, and H. Hochst, J. Vac. Sci. Technol. A **8**, 1577 (1990).
[8] P. R. Pukite, Alex Harwit, and S. S. Iyer, Appl. Phys. Lett. **55**, 2142 (1989).
[9] C. Balasingh, A. Abuhasan, and P. K. Predecki, Powder Diffraction **6**, 16 (1991).
[10] E. A. Stern, Phys. Rev. B **10**, 3027 (1974); F. W. Lytle, D. E. Sayers, and E. A. Stern, *ibid.* **11**, 4825 (1975); E. A. Stern, D. E. Sayers, and F. W. Lytle, *ibid.* **11**, 4836 (1975); P. A. Lee and J. B. Pendry, *ibid.* **11**, 2795 (1975).
[11] For a review see E. A. Stern and S. M. Heald, in *Handbook on Synchrotron Radiation,* edited by D. E. Eastman, Y. Farge, and E. E. Koch (North-Holland, Amsterdam, 1980).
[12] J. Mustre, Y. Yacoby, E. A. Stern, and J. J. Rehr, Phys. Rev. B **42**, 10 843 (1990).
[13] C. Kittel, *Introduction to Solid State Physics,* 6th ed. (Wiley, New York, 1986).
[14] W. H. McMaster, N. Kerr Del Grande, J. H. Mallett, and J. H. Hubbell, *Compilation of X-ray Cross Sections* (National Technical Information Service, Springfield, VA, 1969).

[15]J. K. D. S. Jayanetti, S. M. Heald, and Z. Tan, in *Structure & Properties of Interfaces in Materials,* Symposium Proceedings in the Materials Research Society Vol. 238, edited by W. A. T. Clark, C. L. Briant, and U. Dahman (Materials Research Society, Pittsburgh, 1992).
[16]B. A. Bunker, Ph.D. thesis, University of Washington, 1980.
[17]E. Sevillano, H. Meuth, and J. J. Rehr, Phys. Rev. B **20**, 4908 (1979).
[18]Einstein temperatures Θ_E for the given semiconductors were determined using the experimentally obtained EXAFS Debye-Waller factors, reported in Ref. 16.
[19]Determined using the relationship (Ref. 17), $\Theta_E \simeq 0.75\Theta_D$, where Θ_D is the Debye temperature. Θ_D for metallic Sn was obtained from Ref. 13.
[20]M. Tagaki, J. Phys. Soc. Jpn. **9**, 359 (1954).
[21]C. R. M. Wronsky, Br. J. Appl. Phys. **18**, 1731 (1967).
[22]Ph. Buffat and J-P. Borel, Phys. Rev. A **13**, 2287 (1976).